World Conference on
Timber Engineering
Oslo 2023

EFFECTS OF ELEVATED TEMPERATURE ON BENDING CAPACITY OF STEEL BAR-TIMBER COMPOSITE BEAM

Tsukasa Ueno [1], Nao Matsuoka [2], Shinichi Shioya[3]

ABSTRACT: We have been developing a rigid frame system formed by timber members strengthened by deformed steel bars using epoxy resin adhesive. Buildings may often suffer from elevated temperature in Summer , such as 45.3℃ ever reported in Japan or approximately 65℃ in the attic space. On the other hand, when buildings suffer fire, the composite members also be required to resist against Dead load by using fireproof coating or burning marginal layer (i.e. charring layer). The resisting portion may be mainly lower than 100℃. We planned an experiment to reveal effects of those elevated temperatures on bending capacity of the composite beam. This paper reports the test, its results and discussion.

KEYWORDS: Composite timber, High temperature, Beam, Deformed steel bar, Bending capacity, Fire

1 INTRODUCTION

We have been developing a rigid frame system formed by timber members strengthened by deformed steel bars using epoxy resin adhesive [1]. Buildings may often suffer from elevated temperature in Summer, such as 45.3℃ ever reported in Japan or approximately 65℃ in the attic space. On the other hand, when buildings suffer fire, the composite members also be required to resist against Dead load by using fireproof coating or burning marginal layer (i.e. charring layer). Its portion resisting to dead load will be designed to be mainly lower than 100℃. We planned an experiment to reveal effects of those elevated temperatures on bending capacity of the composite beam. This paper reports the test, its results and discussion.

2 BACKGROUND AND AIM

Little research on heat resistance of timber mixed with different kind of materials, has been reported. Elevated temperatures in building in Japan is such as mentioned above; in an attic space, the maximum temperature may be approximately 75℃. These increase of temperature needs to be considered in design for steel bar(rebar) - timber composite member because of their deference in thermal expansion. We have already revealed creep of the composite beam under elevated temperature of 80-110℃ and reported that the rebar can reduce dramatically the creep of bending deformation of the beam and the proposed method can estimate the creep [2].

However, effects of elevated temperature on bending capacity of the beam were not revealed because of limit of loading apparatus capacity.

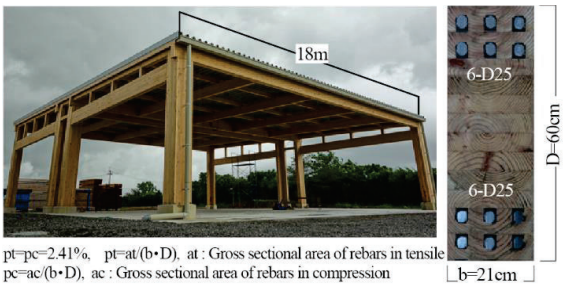

Figure 1: *Prototype building utilizing hybrid beam and column proposed in this study, designed by S. Shioya with approval from authorities and constructed in July 2014*

We planned an experiment of loading the composite beam under the elevated temperatures to reveal the capacity. This paper reports the experimental test and its results.

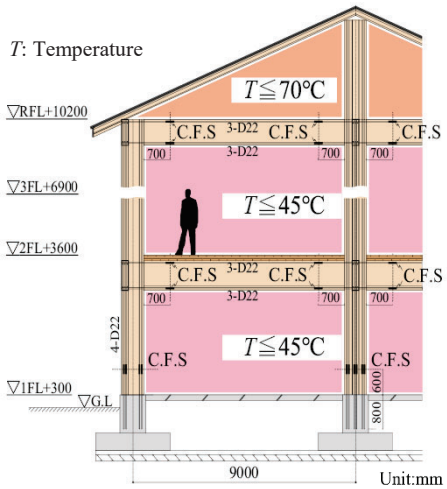

Figure 2: *Elevated temperatures in building assumed in this research*

[1] Tsukasa Ueno, Department of Architecture and Architectural Engineering, Kagoshima University, Japan, k3241487@kadai.jp
[2] Nao Matsuoka, Department of Architecture, Kagoshima University, Japan.
[3] Shinichi Shioya, Department of Architecture, Kagoshima University, Japan, k7347039@kadai.jp

https://doi.org/10.52202/069179-0418

3 EXPERIMENTAL TEST

3.1 SPECIMEN

Figure 3 shows cross-sections of beam specimens which are conventional Glulam timber and the composite timber. Those sizes were adjusted to testing space inside electric heating furnace. Scale ratio of depth of beam was 1/5 and that of width was 1/3 to full-scale beam expected. Area ratios of upper rebar to gross area of beam was 2.54%. The ratio of lower rebar was, also, the same as the upper rebar. Glulam timber employed all low-grade laminas of L50 in Japanese Agriculture Standard to prevent excessive increase in bending capacity because upper limit of the apparatus. The laminas were bonded with resorcinol resin adhesive. Manufacturing process of specimens was the same as that in previous paper [2]. Figure 4 illustrates side views. Furthermore, finger joints were, also, made to be located at its mid-span range in order to prevent excessive increase in load. Properties of rebar, adhesive for rebar, and lamina are listed in Table 1-Table 3.

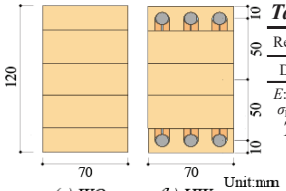

Figure 3: Cross section of beam

Table 1: *Tensile properties of rebar*

Rebar	Grade	E	σ_y	σ_B
D10	SD345	1.96×10^5	403	577

E: Young's modulus, σ_y : Yield strength, σ_B : Breaking strength (Unit: N/mm^2)

Table 2: *Properties of Epoxy adhesive*

E	F_c	F_{cs}
2700	110	60

E: Young's modulus (Unit: N/mm^2)
F_c: Compressive strength
F_{cs}: Shearing strength by compression

Table 3: *Properties of lamina*

Test	Lamina Grade	Lamina Type	The number of testpieces	E in N/mm^2	F_b in N/mm^2
Bending	L50	with joint	5	5501	36.7
		Pure lamina	10	5166	50.3
Tensile		with joint	5	4269	21.9
Compression		Pure lamina	10	4961	32.9

E: Young's modulus, F_c: Bending strength, with joint: testpiec with one finger joint, Pure lamina: testpiec with no finger joint

3.2 SETUP AND LOADING

Figure 4(a) illustrates setup for loading and heating in electric furnace. Photo 1(a) shows loading system against specimen when it is not yet installed within the furnace.; Photo 1(b) shows an outside view of the furnace. The loading was conducted under hanging in mid-air from reaction frame. Specimen was loaded under 4-point bending; upper H-shaped steel beam was subjected to vertical force/F at its mid-span, by oil jack as shown in Figure 4(a) and Photo 1. Shear-span and mid-span lengths were selected so that the specimen will fail in bending.
To prevent the lateral buckling of beam, four steel plates to bind specimen, were connected to the reaction frame, at both supports and near mid span.
Figure 5 shows measuring positions for deformation, strain, and temperature. The deflection at the mid-span was measured with two displacement transducers. The curvature was calculated from foil strain gauges on timber at mid-span and shear strain was done with rosette gauge on both shear spans. Temperatures were measured with thermocouples at three positions: at the top bar, at the bottom bar, and at middle of beam depth.

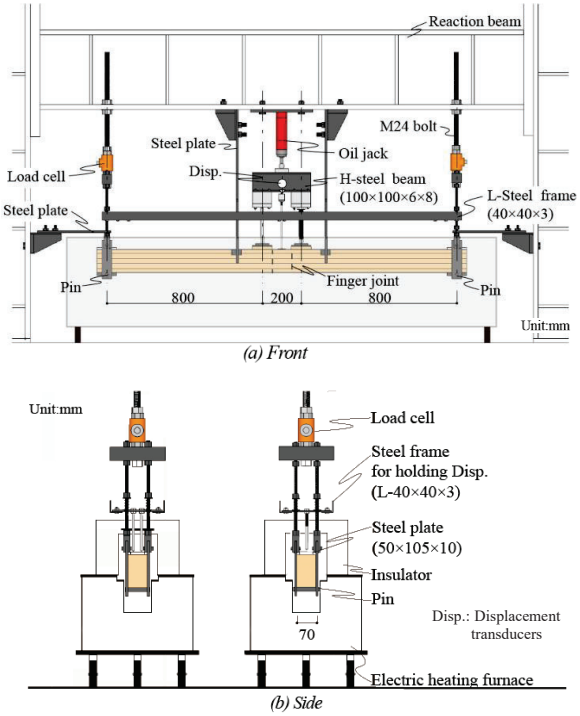

Figure 4: *Setup for loading and heating*

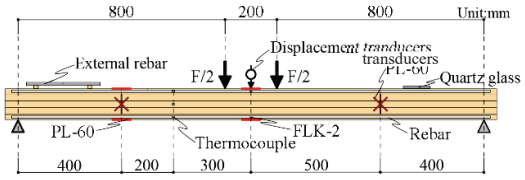

Figure 5: *Arrangement of foil strain gauges and displacement transducers*

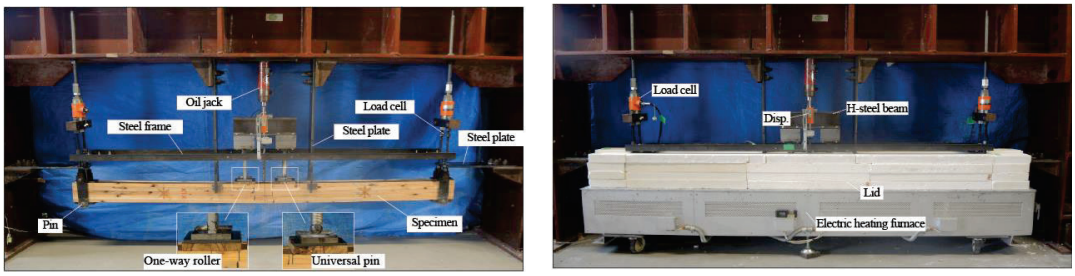

(a)Loading and measuring system after furnace was removed *(b)Heating and loading in electric furnace*

Photo 1: *View of a specimen hanged with bolts connected by loadcell from reaction beam and setup it in furnace*

https://doi.org/10.52202/069179-0418

Table 4: *The number of beam specimen*

Member	Name	Temperature				Total
		RT	45℃	70℃	90℃	
Timber	WO	3	2	2	2	9
Hybrid timber	HW	3	2	3	1	9

RT: Room temperature

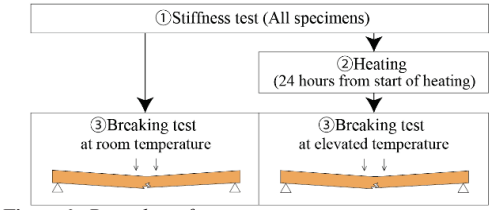

Figure 6: *Procedures for testing*

3.3 HEATING PROGRAM AND TEST PROCEDURE

Table able 4 shows the number of specimens for each target temperature. The temperature levels were assumed as following: room temperature/29.3℃-31.2℃, maximum temperature of the general floor of building/45℃, maximum temperature of the attic of building/70℃, and maximum temperature of steel bar-timber composite beam with fireproof cladding for 2-hour fire resistance/90℃. Figure 6 illustrates procedure for test. First, loading to measure stiffness of each specimen for deflection was conducted at room temperature, and then the specimens were heated up to the target temperature and then was maintained at the temperature for about 24 hours from the start of the heating, and finally, loading was conducted up to fracture under the temperature. On the other hand, unheated specimens were also prepared for loading up to fracture at room temperature. Symbols in the specimen name represents cross section, target temperature, and the order tested within specimens at each target temperature.

3.4 CALIBRATION OF VALUE OF FOIL STRAIN GAUGE

Table 5 lists types of foil strain gauges used for each material. Figure 7 shows condition of gauge attached on test piece of rebar, and Figure 8 shows conditions of foil strain gauge attached on quartz glass with thickness of 10 *mm*. In order to capture behavior of strain gauges due to elevated temperature, strain gauges were attached to quartz glass which is hardly affected by temperature change. In addition, strain change of one external rebar in Figure 7, which was not externally restrained, was prepared for comparison with that of internal rebars within specimen. Quartz glass and external rebar were placed on top of the specimen within the furnace. Only four specimens: HW45-1, HW45-2, HW70-1, and HW70-2 were measured axial strain of the internal rebar. Figure 9 shows behavior of strain gauges attached to the quartz glass as temperature change from the start of heating. The horizontal axis is amount of temperature increase at top of specimen in the furane. As the temperature elevates, the strain of the gauge progresses toward the compression side. This is a characteristic of the strain gauge's self-temperature compensation. The straight line for the data is shown by a pink one dot chain line. The strain value based on the approximate straight line was, in this paper,

Table 5: *Type and measuring length of foil starin gauge*

Material	Type	Length
Rebar	FLK-2	2 *mm*
Timber	PL-60	60 *mm*

Length: measuring length

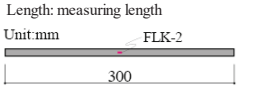

Figure 7: *Location of foil strain gauges on external rebar(D10)*

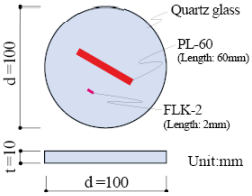

Figure 8: *Foil strain gauges bonded to quartz glass*

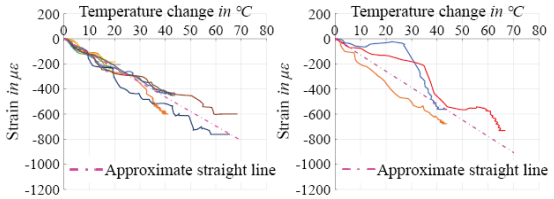

Figure 9: *Foil strain gauge behavior due to elevated temperature*

assumed to be subtracted from value direct-measured on specimen to cancel effect of the self-temperature compensation.

3.5 DIFINITION OF REDUCTION OF MECHANICAL PROPETIES AND ITS EXPRESSION

Effects of moisture content on mechanical properties of wood at elevated temperature was investigated by Kaku and Hasemi et al. by means of bending tests on small specimens of Japanese cedar and zelkova wood [3].

As well as the paper, to investigate effects of temperature rise on mechanical properties of the composite beam, Young's modulus in bending, shear modulus, and bending strength of Glulam timber beam are first expressed as E_{wt}, G_{wt}, and F_{wt}, respectively, with elevated temperature/t. When assuming t=R at room temperature, Young's modulus in bending for Glulam timber beam can be expressed as E_{wR}, E_{w45}, E_{w70}, and E_{w90} at each temperature. Furthermore, residual modulus ration is defined as an index of change in mechanical property with elevated temperature. The residual modulus ratio of Young's modulus/E_{wt} in bending of a Glulam timber beam is expressed as E_{wt}/E_{wR}. Residual modulus ratio of other properties is expressed in the same way.

As Young's modulus in bending and shear modulus can be measured by non-destructive test, E_{wt} and E_{wR}, G_{wt} and G_{wR} can be determined for one same specimen, and the residual modulus ratio can be measured for each specimen. On the other hand, for one same specimen, it is impossible to compare values of bending strength, proportional limit moment, yield moment, and bending strength at different temperatures, for example, 45℃ against room temperature at the same specimen, because the specimen will be subjected up to failure at room temperature.

Therefore, their residual ratios were calculated by dividing experimental value at each target temperature/t by average of an experimental value for specimens that were tested up to failure at room temperature.

https://doi.org/10.52202/069179-0418

Table 6: *Room temperature at starting of heating test* *in ℃*

Specimen	RT			45℃		70℃			90℃	
No.	1	2	3	1	2	1	2	3	1	2
WO	30.8	30.8	29.3	27.7	27.0	30.2	29.6	-	28.2	23.9
HW	31.2	31.0	30.1	26.4	28.8	29.4	29.7	27.3	27.1	-

3.6 HISTROY OF HEATING

Table 6 lists room temperature at the time of the non-destructive stiffness test for each specimen. Figure 10 shows history of heating temperature of specimens. Figure 10(a) and Figure 10(b) are those by thermocouple at upper and lower rebar positions in specimens except HW70-1 and WO70-1; Figure 10(c) is by those of HW70-1 and WO70-1.

For the two specimens shown in Figure 10(c), fluctuating heating was used in order to investigate stress variation in wood and rebar by temperature changing. Heating system of electric furnace caused difference in temperature at upper and lower positions of beam. The temperature in test was controlled by that of thermocouple at upper rebar within specimen.

3.7 EXPERIMENTAL RESULTS

3.7.1 Mechanical properties at room temperature

Table 7 lists experimental results of each specimen by destructive test at room temperature. Figure 11(a) shows moment/M – curvature/ ϕ relationship/M- ϕ for Glulam timber specimen/WORT, Figure 11(b) shows force/F – deflection/δ relationship/F-δ, and Figure 11 (c) shows maximum shear stress/τ_{max} – shear strain/γ relationship /τ_{max} – γ. In Figure 11(a) and (c), average value of three slopes of elastic stiffness is shown by a pink dashed line. Figure 12 shows results for the composite speceimens/HWRT. Averages of experimental bending

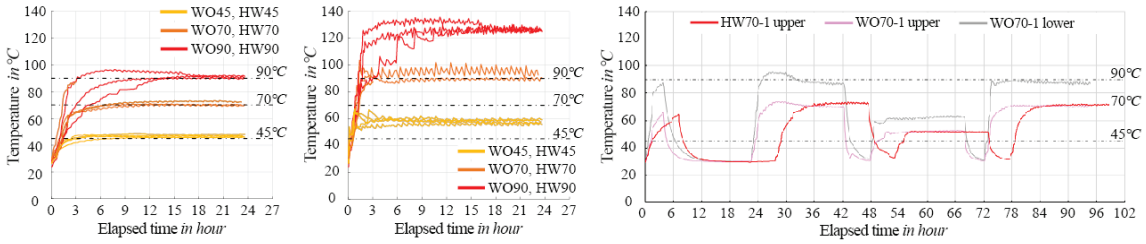

(a) Upper rebar *(b) Lower rebar* *(c) HW70-1 and WO70-1*

Figure 10: *Histories of heating temperature*

Table 7: *Experimental results of specimen at room temperature*

(a) Timber beam

Specimen	E_{wR}	G_{wR}	$E_{wR}\cdot I_{wR}$	$M_{m,wR}$	$F_{b,wR}$
	in N/mm²		*in N·mm²*	*in kN·m*	*in N/mm²*
WORT-1	4266	712	4.30×10^6	4.19	24.97
WORT-2	4993	742	5.03×10^6	4.00	23.80
WORT-3	5357	734	5.40×10^6	3.81	22.69
Average	4872	729	4.91×10^6	4.00	23.82

(b) Steel bar-timber composite beam

Specimen	E_{hR}	G_{hR}	$E_{hR}\cdot I_{hR}$	$M_{p,hR}$	$M_{y,hR}$	$M_{m,hR}$	$F_{b,hR}$
	in N/mm²		*in N·mm²*	*in kN·m*			*in N/mm²*
HWRT-1	4748	806	25.80×10^6	9.23	10.40	13.79	82.07
HWRT-2	4830	876	26.25×10^6	8.65	10.40	13.94	82.95
HWRT-3	4723	923	25.67×10^6	9.10	10.75	13.13	78.17
Average	4767	868	25.91×10^6	8.99	10.52	13.62	81.07

E: Young's modulus, G: Shearing elastic modulus, $E\cdot I$: Bending stiffness, M_p: Bending moment at proportional limit M_y: Yield moment, M_m: Bending moment, F_b: Bending strength

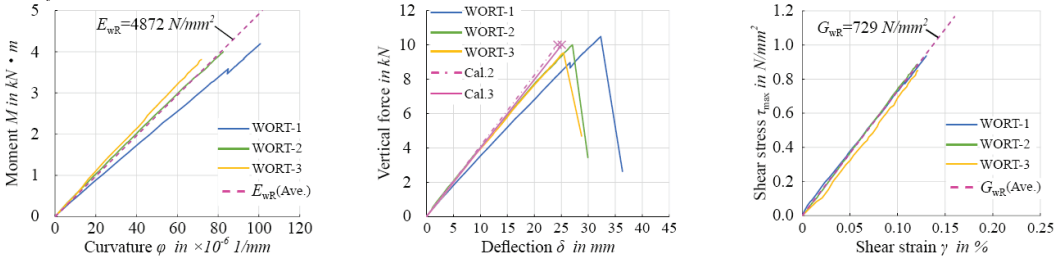

(a) Moment - Curvature of WO *(b) Force - Deflection of WO* *(c)Shear stress - Shear strain of WO*

Figure 11: *Moment - Curvature, Force - Deflection, Shear stress - Shear strain curves of WO at room temperature*

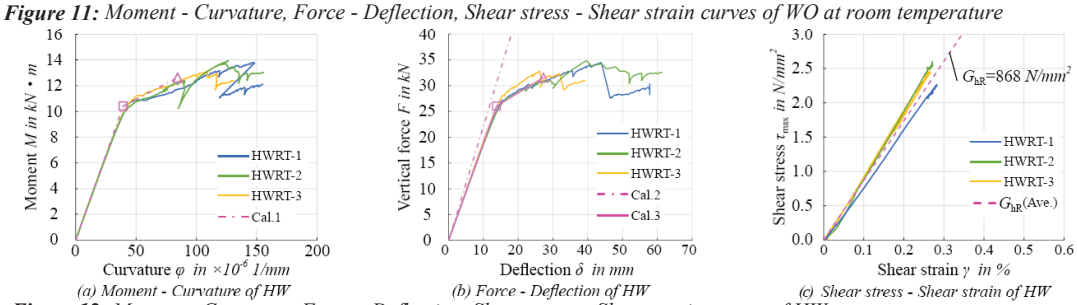

(a) Moment - Curvature of HW *(b) Force - Deflection of HW* *(c) Shear stress - Shear strain of HW*

Figure 12: *Moment - Curvature, Force - Deflection, Shear stress - Shear strain curves of HW at room temperature*

https://doi.org/10.52202/069179-0418

stiffness and bending capacity of the composite specimens/HWRT were 5.28 and 3.40 times higher than those of Glulam timber specimens/WORT, —using Young's modulus of wood in bending of Glulam timber specimen and Young's modulus and yield strength of rebar are shown by a pink one dot chain line by Cal.1 and Cal.2. Calculation process was refered to previus papers[4,5]. Equation for estimation of bending capacity of the composite beam is discribed as following.

$$M_u = {}_wM_u + {}_sM_y \quad (1)$$

where ${}_wM_u$: ultimate moment capcity of timber except the rebars, *i.e.* product of the section modulus and bending strength of timber, ${}_sM_y$: yield moment capacity by only rebar within beam section.

$${}_sM_y = a_t \cdot f_y \cdot j \quad (2)$$

where a_t: gross cross-area of upper or lower rebar
f_y: yield strength of rebar, j: distance from lower the rebar to the upper rebar.

In the composite beam, it can be thought that as yielding and plastic flow occures in rebar befor the beam reaches bending capacity, internal stress due to elevated temperature will decay after its yielding. Therefore Equation (1) can estimate bending capaity of the composite beam by ignoring the internal stress and by considering only decrease of Young's modulus and bending strength of timber owing to elevated temperature. In Figure 11(b) and Figure 12(b), elastic stiffness relationship based on the beam theory (Cal. 2), which considers only flexural deformation is shown by a pink one dot chain line. The relationship (Cal. 3) calculated up to bending fracture by addition of shear deformation is shown by a pink solid line. Point at yield moment is indicated by '□' and point at bending capacity is done by '△'. For shear deformation, a shear modulus of elasticity of 729 *N/mm²* was assumed to be the average of experimental values for Glulam timber specimens /WORT, and the shape factor was assumed to be 1.2 from the energy method for calculating the shear deformation. In the calculated values for the composite specimen, the stiffness of only timber within the composite specimen was assumed to be exhibited, after yielding of rebar. As seen in Figure 12(b), Cal. 3 which considers shear deformation, roughly estimates elastic stiffness, yield moment, secondary stiffness and bending capacity of the composite specimens.

3.7.2 Correction of strain by foil strain gauge

As described in Section 3.4, it is necessary to correct foil strain gauge reading. Figure 13 shows relationship between change in strain of wood and quartz of WO45-1 from heating start and heating elapsed time; Figure 13(a) shows change in measured value, and Figure 13(b) shows change in the corrected value. The time at which target temperature was reached is indicated by black vertical one dot chain line; Figure 14 shows change in strain in wood of HW70-2, and Figure 15 shows change in strain in rebar of the same specimen. Positions and number of the gauge are shown in Figure 16. The strains of wood and rebar need to be corrected on the basis of the approximate straight line shown in Section 3.4 by a pink one dot chain line.

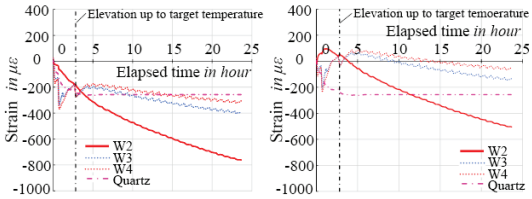

Figure 13: *Strains of wood before and after correction for WO45-1*

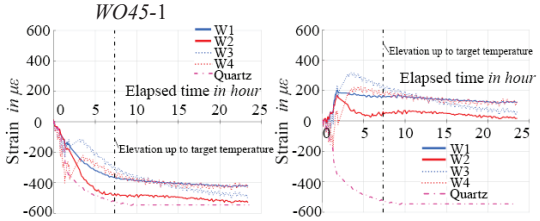

Figure 14: *Strains of wood before and after correction for HW70-2*

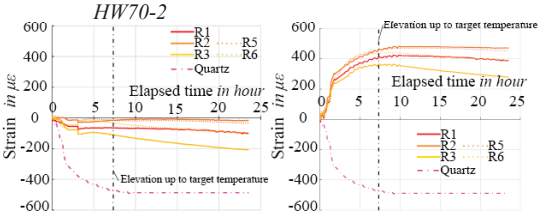

Figure 15: *Strains of rebar before and after correction for HW70-2*

Table 8: *Experimental results of specimen at elevated temperatures represented as average value of each type of specimens*

(a) Timber beam

Specimen	E_{wR}	E_{wt}	$\gamma_{Ew(t)}$	G_{wR}	G_{wt}	$\gamma_{Gw(t)}$	F_{bwt}	$\gamma_{Fbw(t)}$
	in N/mm²		$=E_{wt}/E_{wR}$	*in N/mm²*		$=G_{wt}/G_{wR}$	*in N/mm²*	$=F_{bwt}/F_{bwR}$*
WORT	4872	-	-	729	-	-	23.82*	1.00
WO45	4229	3890	0.92	758	726	0.96	18.80	0.79
WO70	4464	4146	0.93	845	811	0.96	16.80	0.70
WO90	5053	4774	0.95	784	-	-	15.50	0.65

(b) Steel bar-timber composite beam

Specimen	E_{hR}	E_{ht}	$\gamma_{Eh(t)}$	G_{hR}	G_{ht}	$\gamma_{Gh(t)}$	M_{ph}	$\gamma_{ph(t)}$	M_{yh}	$\gamma_{yh(t)}$	M_{mht}	$\gamma_{mh(t)}$	F_{bht}
	in N/mm²		$=E_{ht}/E_{hR}$	*in N/mm²*		$=G_{ht}/G_{hR}$	*in kN·m*	$=M_{pht}/M_{phR}$*	*in kN·m*	$=M_{yht}/M_{yhR}$*	*in kN·m*	$=M_{hmt}/M_{hmR}$*	*in N/mm²*
HWRT	4767	-	-	868	-	-	8.99*	1.00	10.8*	1.00	13.64*	1.00	82.07
HW45	4748	4325	0.91	812	718	0.89	8.20	0.91	9.75	0.90	12.16	0.89	72.38
HW70	4714	4176	0.89	841	775	0.92	8.91	0.99	10.3	0.95	11.48	0.84	68.33
HW90	4808	3815	0.79	886	-	-	6.16	0.69	8.76	0.81	10.28	0.75	61.19

E: Young's modulus
G: Shearing elastic modulus
M_p: Bending moment at proportional limit
M_y: Yield moment, M_m: Bending moment
F_b: Bending strength
γ: Ratios at elevated temperatures

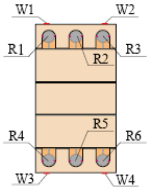

Figure 16: *Gauge's number*

https://doi.org/10.52202/069179-0418

The quartz strain is negative and shrinking over the entire range. This means effect of the self-temperature compensation of foil strain gauge. Measured strains of wood and rebar are negative as the temperature rises, but the corrected strains of wood and rebar are positive until the target temperature was reached, which can be explained by phenomenon of thermal expansion of material. By using the corrected values of strain, discussion hereafter is done.

3.7.3 Degrade in mechanical properties with elevated temperature

Table 8 in the previous page lists mechanical properties and the residual modulus ratios from the loading tests. Figure 17 shows comparison of moment-curvature and force-deflection relationships for Glulam timber specimen and composite specimen. Numbers in the figures indicate the number of specimen name. Compared to Glulam timber specimen, the composite specimen maintained extremely high stiffness and bearing capacity even at high temperatures. Stiffness and bending capacity of both the Glulam timber specimen and the composite specimen decreased with elevated temperature, against those at room temperature.

Figure 18 shows variation of residual modulus ratio of the initial bending stiffness. Coloured symbols indicate experimental values for the composite specimen; uncoloured symbols indicate those for the Glulam timber specimen. Red solid line and blue solid line indicate average of those experimental values for each type, respectively.

The residual modulus ratio of initial stiffness in bending of Glulam timber shown in Figure 18 hardly decrease above 45°C and increases at 90°C. This tendency is also observed in the residual modulus/$\gamma_{wG(t)}$ and $\gamma_{hG(t)}$ of elasticity in shear, as seen in Table 8 (a) and (b).

It is considered that moisture in wood might have been removed as temperature rising and this phenomenon would mitigate the decrease in stiffness.

On the other hand, it should be noted that the residual modulus ratio of bending stiffness of the composite beam

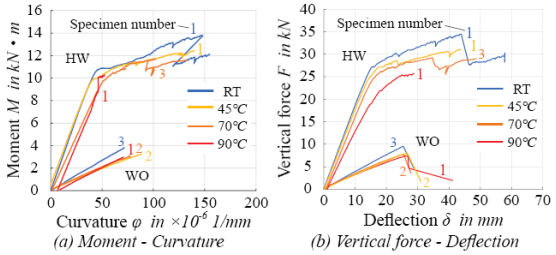

Figure 17: *Comparison of experimental property at each temperature*

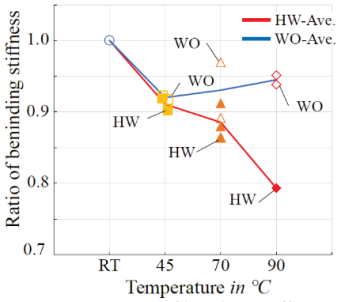

Figure 18: *Ratio of bending stiffness at elevated temperature to stiffness at room temperature*

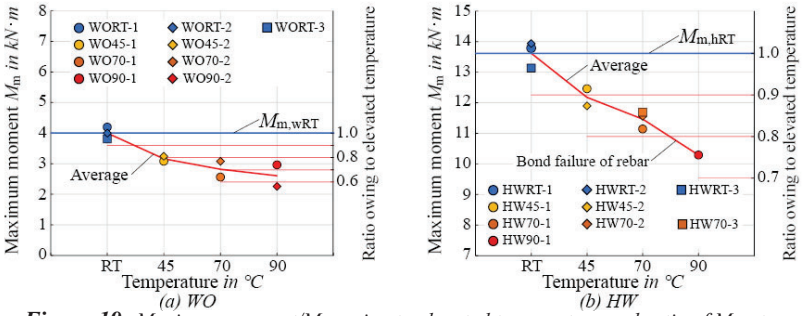

Figure 19: *Maximum moment/M_m owing to elevated temperature and ratio of M_m at elevated temperature to $M_{m,RT}$ at room temperature*

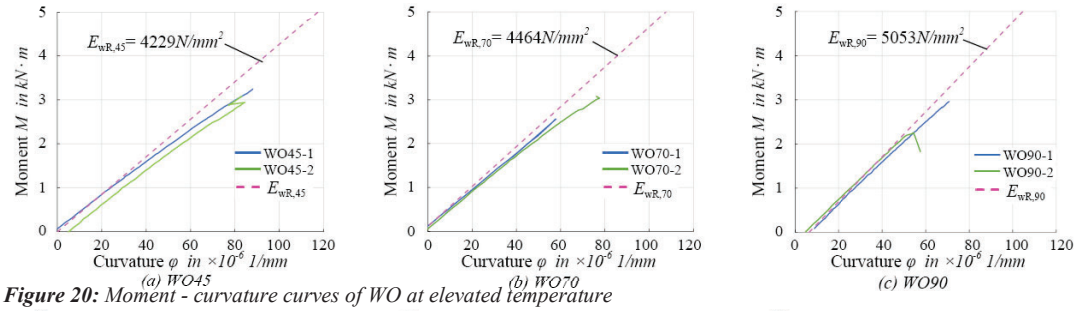

Figure 20: *Moment - curvature curves of WO at elevated temperature*

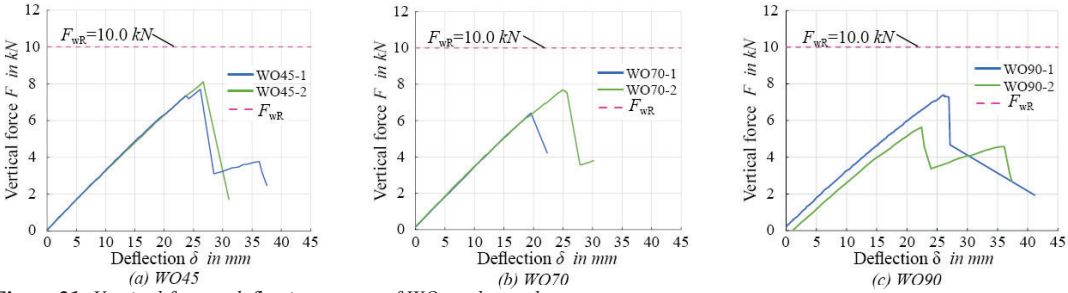

Figure 21: *Vertical force - deflection curves of WO at elevated temperature*

https://doi.org/10.52202/069179-0418

decreased as temperature rising as seen in Figure 18. In addition, the performance of rebar bonded in timber under high temperature might have decayed due to softening of the adhesive of rebar at elevated temperature.

Figure 19 shows variation of the residual ratio of bending capacity. Compared to Glulam timber specimen, the composite specimen performed a smaller percentage loss of performance. The decrease was more pronounced as temperature rising in both specimen types. It can be confirmed that the decrease in bending capacity of the composite specimens is limited to be 20% or less at temperatures below 70°C. Figure 20 shows moment-curvature relationship for Glulam timber specimen at elevated temperatures. Pink dashed line is average of bending stiffness at room temperature. Figure 21 shows force-deflection relationship of Glulam timber specimen at different temperatures. Horizontal pink dashed line is average of maximum force of the Glulam timber specimen/WORT at room temperature. Stiffness and maximum capacity of the Glulam timber specimen is seen to decrease at elevated temperatures compared to room temperature.

3.7.4 Failures after loading test

Figure 22 shows failures of specimens after destructive loading test. All specimens showed tensile fracture at lower portion of wood near mid-span. Those cracks progressed from finger joints. For the Glulam timber specimens, there was no significant difference in failure between at room temperature and at 90°C. On the other hand, for the composite specimens, bond failure around lower rebar was observed in addition to the finger joint fracture in HW90-1. The fracture is shown in Figure 22(d), (e), and Photo 2. Its Cracks were observed along the lower rebar in the axial direction of it. This failure was not observed in the other composite specimens. The upper temperature limit of the epoxy adhesive for bonding rebar is 110°C based on the results of a push-through test under elevated temperature [5]. As shown in Figure 10(a) and (b), owing to heating system of electric furnace, temperature at

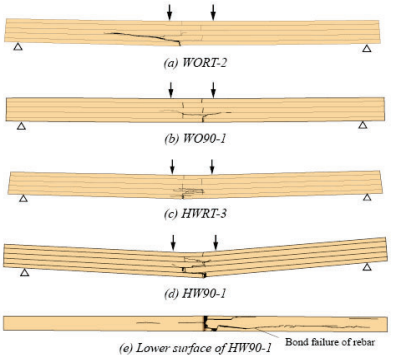

Figure 22: *Failures of specimens after loading test*

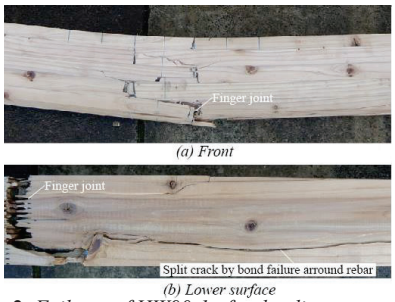

Photo 2: *Failures of HW90-1 after loading test*

position of the lower rebar exceeds 120°C when heated to 90°C at the upper rebar. The excessive temperature rising might have resulted in a decrease in rigidity of Epoxy adhesive around the lower rebar.

3.7.5 Estimation of mechanical properties of composite beam

Figure 23 and Figure 24 show moment-curvature and force-deflection relationships of the composite specimens at different temperatures, respectively.

As curvature, deflection, and strain were generated during heating, there was a residual component due to its heating at the start of loading immediately after heating program was completed.

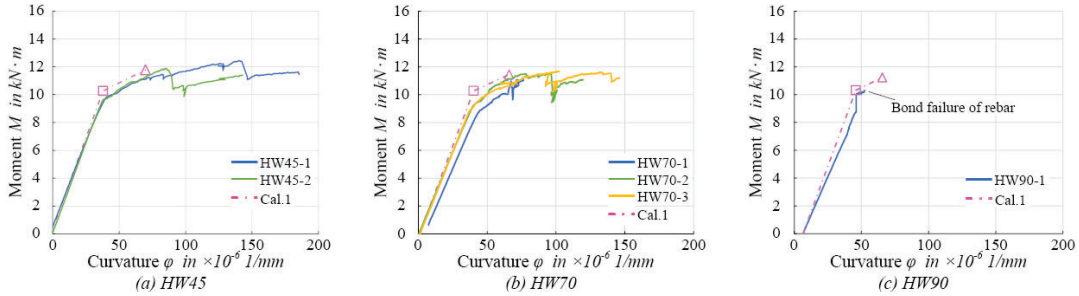

Figure 23: *Moment - curvature curves of HW at elevated temperature*

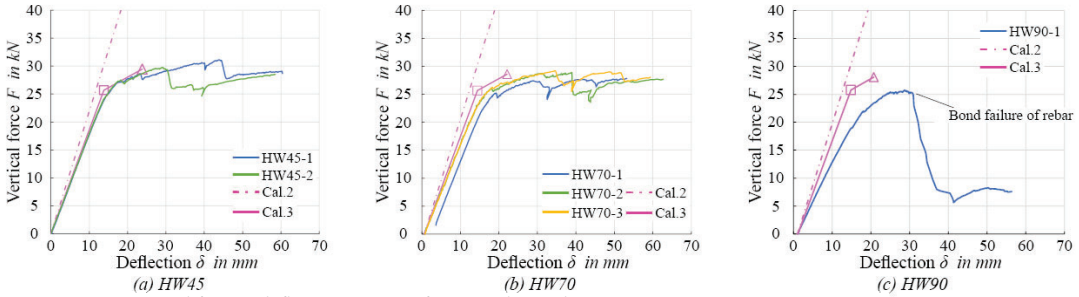

Figure 24: *Vertical force - deflection curves of HW at elevated temperature*

https://doi.org/10.52202/069179-0418

Cal.1, Cal.2 and Cal.3 in the same figure are the same as those in Section 3.7.1, but as modulus of elasticity and bending strength of timber decrease with elevated temperature, the decrease ratios were considered in the calculation. In Figure 24, except for the bending strength at 90°*C*, the bending stiffness and bending capacity are generally estimated by the calculated values.

On the other hand, the variation of temperature and moisture content might have caused internal stress and decreased the yield moment. The fact that none of the calculated values considers the amount of variation in the stress may have resulted in overestimation of yield moment. In Figure 23(c) and Figure 24(c), those of the specimen at 90°*C* have overestimated bending capacity. As mentioned above, bond stiffness around rebar is considered to have decreased with the elevated temperature. The decrease in bond stiffness is considered to have led to a decrease in bending capacity because contribution of the rebar is reduced.

Figures 25(a) and (b) show moment-strain relationships for wood and rebar of the composite specimens during stiffness tests at 45°*C*. Figures 25(c) and 25(d) and 25(e) and 25(f) show moment-strain relationships at 45°*C* and 70°*C*, respectively, during destructive loading. Solid yellow and red lines represent strain of upper and lower surface of timber and strain of rebar, respectively, calculated based on the assumption of plane of cross-section. To the increased strain by loading, the residual strain after the heating was added. In calculated values, degradation of wood's performance due to elevated temperature was considered. In the figure, '□' is experimental strain of wood and ○ is experimental strain of rebar. For 70°*C*, experimental value of wood strains on the bending-tension side were larger than the calculated values. Temperature at lower rebar position reached 90°*C* or higher when heated at 70°*C* as reason of electric furnace mentioned above. This is considered to cause a decrease in wood performance or adhesion stiffness. The horizontal pink dashed line in the figure represents calculated yield moment. This calculated value is the same as '□' symbols shown in Figures 23 and 24, which only consider the reduction in wood performance. As mentioned above, it can be seen here that the calculated values provided an overestimation of yield moment.

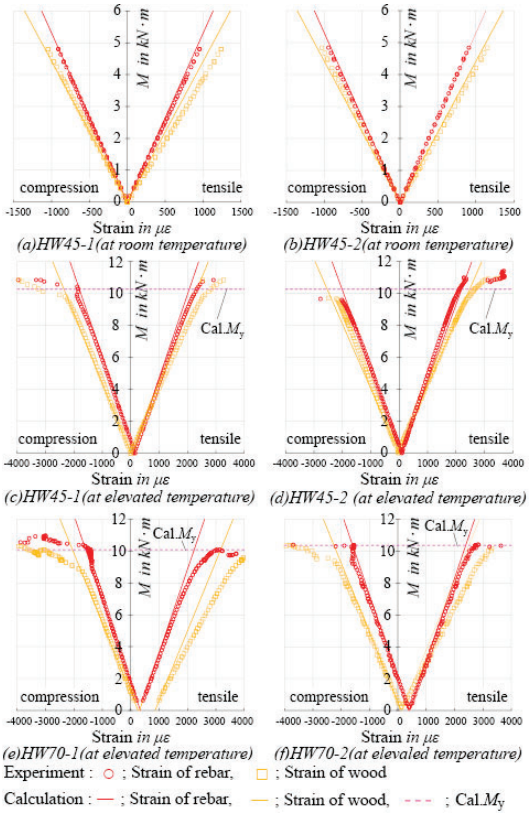

Figure 25: *Comparison of calculation to experiment of bending moment-strain curves on rebar and timber surface*

3.7.6 Strain of rebar outside and wood within specimen

Figure 26 and Figure 27 show variations of strains of external rebar and surface of timber with heating time passing. Timing at which is reached the target temperature is represented by a vertical one dot chain line. In WO45-1, the gauge at point W1 on the upper surface of beam was defective. Strain on the external rebar was almost constant after it reaching target temperature. Assuming that coefficient of thermal expansion of rebar is 10 μ/°C, i.e., a common value, amount of the coefficient multiplied by the amount of temperature increased from initial temperature of heating is shown by thin blue line/Cal.R.

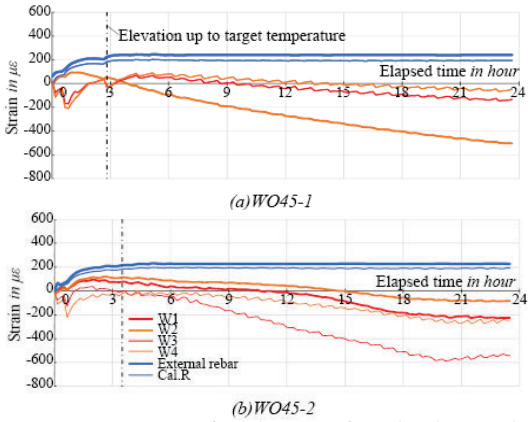

Figure 26: *Variation of axial strains of wood and external rebar in WO45-series specimen heated up to 45 °C*

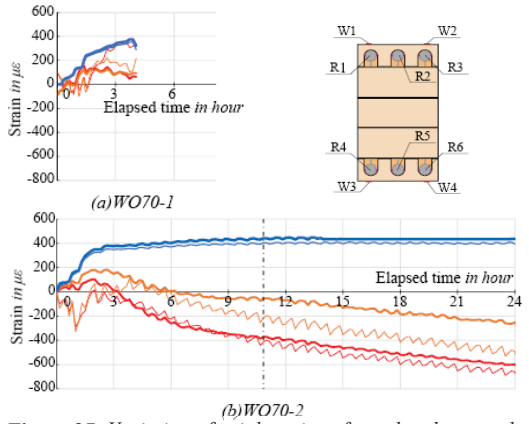

Figure 27: *Variation of axial strains of wood and external rebar in WO70-series specimen heated up to 70 °C*

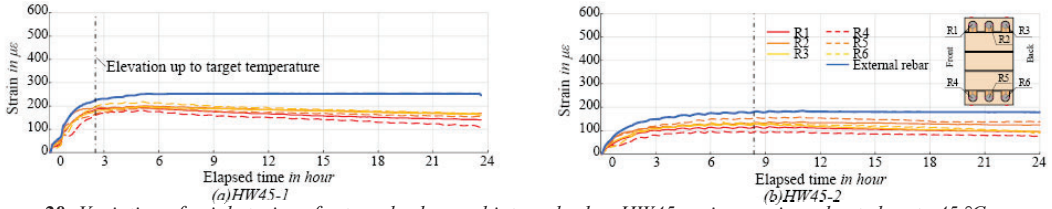

Figure 28: *Variation of axial strains of external rebar and internal rebar HW45-series specimen heated up to 45 ℃*

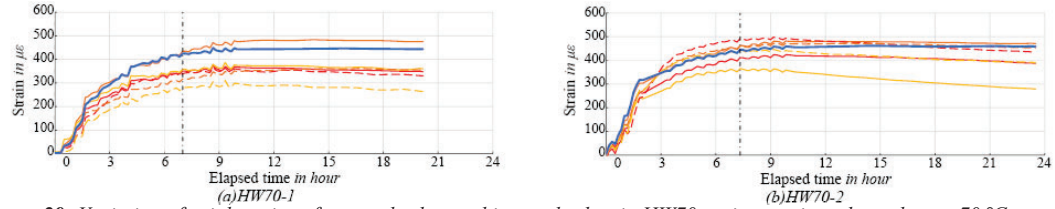

Figure 29: *Variation of axial strains of external rebar and internal rebar in HW70-series specimen heated up to 70 ℃*

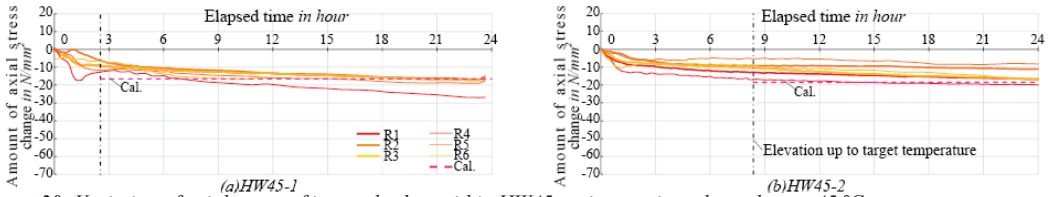

Figure 30: *Variation of axial stress of internal rebar within HW45-series specimen heated up to 45 ℃*

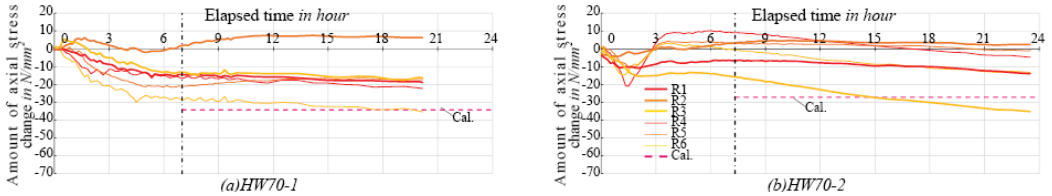

Figure 31: *Variation of axial stress of internal rebar within HW70-series specimen heated up to 70 ℃*

As the external rebar was located on the upper surface of specimen, temperature at the upper rebar was assumed to be temperature of the external rebar. For heating temperatures of 45°*C* and 70°*C*, amounts of elongation strain (thick blue line) of the external rebar generally agreed with the calculated values (thin blue line) of the elongation strain of the external rebar.

On the other hand, strain of wood in Glulam timber specimens increased positive at the beginning of heating, but began to decrease before the target temperature was reached, and then became negative and shrank after the target temperature was reached. This phenomenon is considered to be caused by dehumidification of wood during heating and shrinkage in grain direction of wood because humidity was not controlled in the electric furnace. This is more pronounced at the higher heating temperature of 70°*C*. It can be confirmed that shrinkage due to decrease in moisture content is larger than thermal expansion of wood due to elevated temperature. This suggests that internal stresses in attic of actual buildings need to be estimated taking into account both the shrinkage of wood due to decrease in moisture content and elongation of rebar due to increase in temperature, because of repeative high temperature environment in the attic.

3.7.7 Strain of rebar within specimen

Figure 28 and Figure 29 show variations of strains of the external rebar and the internal rebar. The point at which it reached the target temperature as well, is indicates by a vertical one dot chain line. For the specimens at 45°*C*, strain of the internal rebar was smaller than that of the external rebar, and strains of upper and lower bars were similar. In HW70-1 at 70°*C*, strain of internal rebar was also smaller than that of the external rebar, but in HW70-2, strains of the external and internal rebars were close. As strain of the external rebar was stable at the same level in the two specimens, it is considered that variation of wood may have some influence, but the increase in strain of internal rebar in HW70-2 cannot be explained. The reason for the smaller strain in the internal rebar relative to the external rebar is that the internal rebar is restricted by wood around itself. All strains of the internal rebar decreased as heating time passing. No such decrease occurs in the external rebar. Therefore, the decrease in strain of the internal rebar can be attributed to the shrinkage of timber due to the dehumidification of wood.

3.7.8 Stress of internal rebar based on strains of external rebar and timber

Figure 30 and Figure 31 show variation of amount of axial stress of rebars in the composite specimens during heating. The amount of stress variation is the amount of variation of the difference in strain between the external and the internal rebar in Figure 28 and Figure 29 multiplied by Young's modulus of rebar (experimental value). Equation (3) shows an equation for estimation of yield moment.

https://doi.org/10.52202/069179-0418

$$M_y = \sigma_y / n(I_e / y_s) \quad (3)$$

where y_s: distance from the neutral axis to rebar, σ_y: yield strength of rebar, n: ratio of Young's modulus of rebar to bending Young's modulus of timber, I_e: sectional secondary moment considering rebar

Equation (3), which estimates yield moment when the rebar yields, is affected by ratio/n of Young's modulus in bending between rebar and timber. As shown in Table 1, Young's modulus of timber in bending with increasing temperature was captured by force tests on Glulam timber specimens. Using Young's modulus from non-destructive test before heating and Young's modulus from loading after heating test, yield moments in each case are calculated using Equation (3), and difference between the former and latter calculated values may be regarded to be component of yield moment due to only the reduction in Young's modulus of timber.

Figure 32 shows variation of calculated yield moment with increasing temperature as indicated by pink dashed line/Cal.M_y, where Cal.M_y can be seen to estimate experimental value of HWRT at room temperature.

Average of the experimental values at room temperature is shown by a blue horizontal line/$M_{y,hRT}$.

Difference of Cal.M_y with respect to $M_{y,hRT}$ means amount due to the reduction of Young's modulus in bending of timber. Magnitude of those difference ranges only 4-8% of calculated yield moment at room temperature. The difference between Cal.M_y and experimental value indicated by red solid line means amount due to the difference in expansion and contraction between rebar and timber.

The reduction/ΔM in moment can be evaluated by replacing yield stress/σ_y in Equation (3) with amount /$\Delta\sigma_T$ of increase or decrease in axial stress of rebar, and the equation can be given as Equation (4).

$$\Delta M = \Delta\sigma_T / n(I_{eT} / y_s) \quad (4)$$

$\Delta\sigma_T$ in Equation (4) can be back-calculated by ΔM. Assuming that ΔM is equal to amount of Cal.M_y subtracted by average values of experimental yield moments at each temperature, $\Delta\sigma_T$ can be obtained by using Equation (4).

Results of $\Delta\sigma_T$ calculated are shown in Figure 30 and Figure 31 by horizontal a pink dashed line (Cal.). Cal. estimated roughly the experimental value of stress in internal rebar in HW45-1 and 2, but, in HW70-1 and 2, Cause of tend to overestimate those in compression is unknown currently.

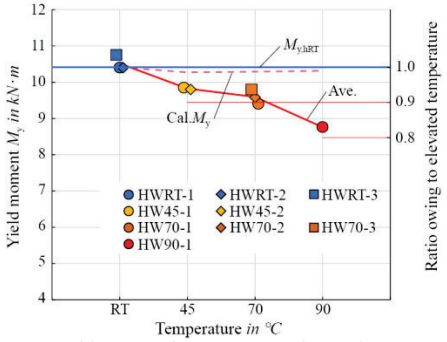

Figure 32: *Yield moment/M_y owing to elevated temperature and ratio of M_y at elevated temperature to $M_{y,RT}$ at room temperature*

On the basis of above discussion, equation for estimation of yield moment of steel bar-timber composite beam that takes temperature rise into account can be summarized as following.

$$M_y = (\sigma_y - \Delta\sigma_T) / n(I_{eT} / y_s) \quad (5)$$

where σ_y, $\Delta\sigma_T$, y_s: previous definition, n_T: ratio of Young's modulus of rebar to Young's modulus of timber in bending at elevated temperature, I_{eT}: cross-sectional secondary moment of the composite beam considering elevated temperature

In the future, it is necessary to estimate variation of the internal stress of rebar.

4 SUMMARY

Bending test of beams under high temperature with uncontrolled moisture absorption and dehumidification of wood were conducted to investigate effect of temperature rising on mechanical properties of the steel bar-timber composite beam. The results are summarized as the followings:

i) Although Young's modulus in bending, shear modulus and bending strength of timber decrease with temperature rising, the decrease is mitigated by loss of moisture in timber.

ii)Bending stiffness and bending capacity of the composite beam could be estimated from room temperature to 70°C, by the proposed estimation method considering the decrease in Young's modulus and bending strength of timber due to temperature rising, ignoring internal stress caused by the temperature.

iii) Yield moment of the composite beam should take into account effect of the internal stress in addition to decrease in mechanical performance of timber owing to temperature rising. In the future, we plan to develop a method for estimating the internal stress on safe side.

ACKNOWLEDGEMENT

This project was funded by Grant-in-Aid for Challenging Research in Japan and its experiment was conducted by all staffs of Shioya's laboratory. The authors gratefully acknowledge their work.

REFERENCE

[1] S.Shioya, et al.: An innovative hybrid timber structure in Japan: performance of column and beam, Vienna, WCTE 2016.

[2] N. Matsuoka, K. Fukudome, S. Shioya: Heat resistance of steel bar -timber composite beam, Santiago, WCTE 2021.

[3] C. Kaku, Y. Hasemi, et al.: Influence of moisture content on the structural properties of wood under high temperature, Vienna, WCTE 2016.

[4] N. Fukutomi, S. Shioya: Design method to estimate stiffness and strength of hybrid timber-steel bar beams, Seoul, WCTE 2018

[5] Mori, S. Shioya: Stiffness and strength of full-scale steel bar-timber composite beams with comparative small-depth, Santiago, WCTE 2021